J|A|C|S
ARTICLES
Published on Web 03/21/2006

Nanostructuration of Phenylenevinylenediimide-Bridged Silsesquioxane: From Electroluminescent Molecular J-Aggregates to Photoresponsive Polymeric H-Aggregates

Olivier J. Dautel,*,† Guillaume Wantz,‡ Robert Almairac,# David Flot,§ Lionel Hirsch,‡ Jean-Pierre Lere-Porte,† Jean-Paul Parneix,‡ Françoise Serein-Spirau,† Laurence Vignau,‡ and Joël J. E. Moreau*,†

Contribution from Hétérochimie Moléculaire et Macromoléculaire UMR CNRS 5076, Ecole Nationale Supérieure de Chimie de Montpellier, 8 rue de l'Ecole Normale 34296 Montpellier Cedex 05, France, Fédération de Recherche CNRS FR2648 - Laboratoires PIOM & IXL, Ecole Nationale Supérieure de Chimie et de Physique de Bordeaux, 16 Av. Pey Berland 33607 Pessac Cedex, France, LCVN, UMR 5587, cc26 Université Montpellier II, 34095 Montpellier Cedex 05, France, and European Molecular Biology Laboratory 6, rue Jules Horowitz, BP181, 38042 Grenoble Cedex 9, France

Received January 3, 2006; E-mail: joel.moreau@enscm.fr; olivier.dautel@enscm.fr

Abstract: A new approach to control molecular aggregation of π-conjugated chromophores in the solid state has been investigated. Our strategy was to use a modifiable bulky fragment which should induce a J-aggregation and offer the possibility to reach an H-aggregation upon its chemical modification by lateral slip of π-conjugated molecules. The chosen fragment for that purpose was the hydrolyzable triethoxysilane function ($Si(OEt)_3$). Our objective was to design and synthesize electroluminescent or solar cell hybrid organic−inorganic materials by the sol−gel process applied to a bifunctionalized silane. With this intention, the synthesis of the sol−gel processable phenylenevinylenediimide silsesquioxane **6** was accomplished and the study of spin-coated thin films of the pure silane precursor subjected or not to the sol−gel process has been carried out. Optical properties of **6** are consistent with the formation of J-aggregates in the solid state due to the steric hindrance introduced by the triethoxysilane units. Conversely, the spectroscopic behavior observed for the hybrid film **6F** is attributed to an H-aggregation corresponding to a "card pack" orientation of the distyrylbenzeneimide chromophores in the compressed silicate network. Morevover, **6** and **6F** also exhibited different electronic behaviors: light-emitting diodes exhibited high brightness with the native precursor **6** and almost no light output with the sol−gel processed silsesquioxane **6F**. Photovoltaic cells showed the opposite behavior with low photocurrent generation in the precursor case and higher photocurrents with the sol−gel processed layers. These results provide a deeper understanding of the present self-assembly process that is strongly governed by the molecular packing of the oligosiloxane precursor.

Introduction

Electronically active organic polymers are of great interest for electronic devices because of their low processing costs and their desirable mechanical properties.[1] During the past decade, several polymeric materials suitable for light-emitting devices have been developed.[2] The basic requirement is a highly efficient luminescent material with good thermal and photochemical stabilities. In this context, we recently described the optical and electroluminescent properties of a new chiral electroluminescent polyimide consisting of alternating conjugated segments and chiral units. The synthesized polymer exhibited high thermal stability, high electron affinity, and good thin-film forming ability. The C_2 symmetry of the chiral unit induces a secondary structure which reduces all types of intra- and interchain interactions. The incorporation of a well-defined phenylene-ethynylene substructure within the chiral backbone allowed the fabrication of a monolayer electroluminescent polymeric diode with higher performances than the related isolated imidophenyleneethynylene (ImPE) (Scheme 1).[3]

This type of conjugated polymer has desirable mechanical properties, but the lack of long-range interchain order reduces performance. As a result, the detailed understanding of the supramolecular interactions between the individual π-conjugated molecules has become one of the most challenging scientific research areas. Indeed, for electronic devices made out of π-conjugated molecules, it is a real challenge to obtain monodomainly ordered structures in the micrometer regime.[4] The

† Ecole Nationale Supérieure de Chimie de Montpellier.
‡ Ecole Nationale Supérieure de Chimie et de Physique de Bordeaux.
# cc26 Université Montpellier II.
§ European Molecular Biology Laboratory 6.

(1) Skotheim, T. A.; Elsenbaumer, R. L.; Reynolds, J. R. *Handbook of Conducting Polymers*; Marcel Dekker Inc., New York, 1998.
(2) Burroughes, J. H.; Bradley, D. D. C.; Brown, A. R.; Marks, R. N.; Mackay, K.; Friend, R. H.; Burn, P. L.; Holmes, A. B. *Nature* **1990**, *347*, 539−541.
(3) Dautel, O. J.; Wantz, G.; Flot, D.; Lere-Porte J.-P.; Moreau, J. J. E.; Parneix, J.-P.; Serein-Spirau, F.; Vignau, L. *J. Mater. Chem.* **2005**, *15*, 4446−4452.

10.1021/ja058680z CCC: $33.50

Scheme 1. Incorporation of a Well-Defined Oligo-phenyleneethynylene Substructure within a Chiral Backbone

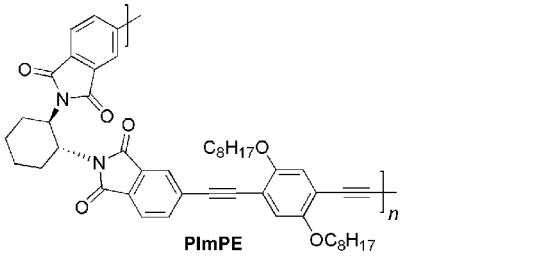

PImPE

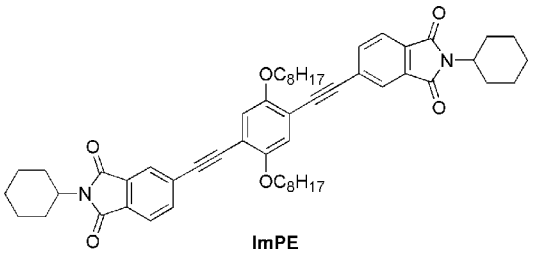

ImPE

recent strategies of self-assembly and supramolecular chemistry are interesting alternatives for the bottom-up design of organic devices.[5] Controlled aggregation of π-conjugated systems offers interesting electronic and photonic functional materials that are different from their monomeric state. The self-association of chromophores in the solid or at the solid−liquid interface is a frequently encountered phenomenon in dye chemistry owing to strong intermolecular van der Waals-like attractive forces between molecules. The aggregates in the solid state exhibit distinct changes in the absorption band as compared to the monomeric species.[6] From the spectral shifts, various aggregation patterns of the dyes in different media have been proposed. The bathochromically shifted J-bands[7] and hypsochromically shifted H-bands[8] of the aggregates have been explained in terms of molecular exciton coupling theory, i.e., coupling of transition moments of the constituent dye molecules.[9] It is generally agreed that both H- and J-aggregates are composed of dye molecules stacked in a parallel way. A plane-to-plane stacking results in a sandwich-type arrangement (H-aggregates) whereas a head-to-tail arrangement forms J-aggregates leading to two-dimensional dye crystals. From Figure 1, it can be postulated that going from a J-aggregation to an H-aggregation will improve the intermolecular overlaps increasing the charge transport properties. Furthermore, since the corresponding total transition dipole moment vanishes, H-aggregates are generally considered as poor emitters.[10] Thus, the aggregation pattern of π-conjugated oligomers will determine the device performance and/or goal i.e. OLED or solar cells. In other words, it should be possible using the same electroactive molecule to tune itsoptoelectronic properties by simply playing on the modulation of its aggregation.

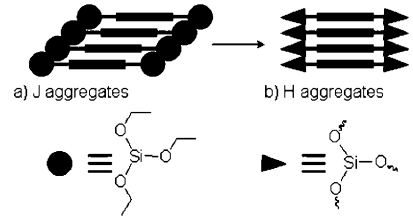

Figure 1. New strategy to go from a J- to an H-aggregation.

The tendency of molecules to aggregate depends on the structure of the chromophore and also on its environment. However, the rational control of a dye aggregation is still difficult because molecules tend to spontaneously align themselves into a one-dimensional infinite aggregate in a face to face manner by means of π-stacking and/or van der Waals interactions. The development of a method to control their aggregation behavior and orientations is a challenge.

In this context, we developed a new family of oligophenylenevinylene derivatives incorporating conjugated imide functions (ImPV) (Scheme 2). These functions are thermally and chemically stable. Their electron affinity confers to the whole molecule the electron transport properties which are lacking to the phenylenevinylene moiety. This novel bisimidophenylenevinylene (ImPV) derivative has been chosen for this study because this material exhibits acceptable performances even in single layer OLED.[11]

In the first part of this manuscript, the relation between the supramolecular organization of ImPV and its optoelectronic properties will be studied. Our approach toward the control of its supramolecular organization and its optoelectronic properties will be then described.

Our strategy to control its aggregation behavior and orientations was to use a modifiable bulky fragment which should cause a lateral slip of molecules from a J-aggregation to an H-aggregation upon its chemical modification (Figure 1). The fragment chosen for that purpose was the hydrolyzable triethoxysilane function ($Si(OEt)_3$). Hybrid silicate materials derived from the hydrolytic polycondensation of organo-bridged silsesquioxane precursors, $(RO)_3-Si-R'-Si-(OR)_3$, where R and R′ are organic groups, have received increasing attention over the past decade.[12−15] Recently, efforts have been made to better control their structure to create new functional materials. Several groups reported on the covalent introduction of oligo-1,4-phenylenevinylene (OPV) segments in silica sol−gel systems.[16]

(4) (a) Kläerner, G.; Müeller, M.; Morgenroth, F.; Wehmeier, M.; Soczka-Guth, T.; Müellen, K. *Synthetic Metals* **1997**, *84*, 297−301. (b) Salzner, U. *Curr. Org. Chem.* **2004**, *8*, 569−590.
(5) Hoeben, F. J. M.; Jonkheijm, P.; Meijer, E. W.; Schenning, A. P. H. J. *Chem. Rev.* **2005**, *105*, 1491−1546.
(6) Mishra, A.; Behera, R. K.; Behera, P. K.; Mishra, B. K.; Behera, G. B. *Chem. Rev.* **2000**, *100*, 1973−2012.
(7) (a) Jelly, E. E. *Nature* **1936,** *138*, 1009−1010. (b) Scheibe, G. *Angew. Chem.* **1936**, *49*, 563.
(8) Brooker, L. G. S.; White, F. L.; Heseltine, D. W.; Keyes, G. H.; Dent, S. G.; VanLare, E. J. *J. Photogr. Sci.* **1953**, *1*, 173−183.
(9) (a) McRae, E. G.; Kasha, M. *J. Chem. Phys.* **1958**, *28*, 721−722. (b) Kasha, M.; Rawls, H. R.; El-Bayoumi, M. A. *Pure Appl. Chem.* **1965**, *11*, 371−392.
(10) Davydov, A. S. *Theory of Molecular Excitons*; Plenum: New York, 1971.
(11) Wantz, G.; Dautel, O. J.; Almairac, R.; Hirsch, L.; Serein-Spirau, F.; Vignau, L.; Lee-Porte, J.-P.; Parneix, J. P.; Moreau, J. J. E. *Org. Electron.* **2005**, *7*, 38−45.
(12) (a) Shea, K. J.; Loy, D. A.; Webster, O. W. *J. Am. Chem. Soc.* **1992**, *114*, 6700−6710. (b) Corriu, R. J. P.; Moreau, J. J. E.; Thepot, P.; Wong Chi Man, M. *Chem. Mater.* **1992**, *4*, 1217−1224.
(13) (a) Kapoor, M. P.; Yang, Q.; Inagaki, *S. J. Am. Chem. Soc.* **2002**, *124*, 15176−15177. (b) Guan, S.; Inagaki, S.; Ohsuna, T.; Terasaki, O. *J. Am. Chem. Soc.* **2000**, *122*, 5660−5661. (c) Inagaki, S.; Guan, S.; Ohsuna, T.; Terasaki, O. *Nature* **2002**, *416*, 304−307. (d) Lu, Y.; Fan, H.; Doke, N.; Loy, D. A.; Assink, R. A.; LaVan, D. A.; Brinker, C. J. *J. Am. Chem. Soc.* **2000**, *122*, 5258−5261.
(14) (a) Moreau, J. J. E.; Vellutini, L.; Wong Chi Man, M.; Bied, C.; Bantignies, J.-L.; Dieudonne, P.; Sauvajol, J.-L. *J. Am. Chem. Soc.* **2001**, *123*, 7957−7958. (b) Moreau, J. J. E.; Pichon, B. P.; Wong Chi Man, M.; Bied, C.; Pritzkow, H.; Bantignies, J.-L.; Dieudonne, P.; Sauvajol, J.-L. *Angew. Chem., Int. Ed.* **2004**, *43*, 203−206.
(15) (a) Liu, N.; Yu, K.; Smarsly, B.; Dunphy, D. R.; Jiang, Y.-B.; Brinker, C. J. *J. Am. Chem. Soc.* **2002**, *124*, 14540−14541. (b) Barboiu, M.; Cerneaux, S.; van der Lee, A.; Vaughan, *G. J. Am. Chem. Soc.* **2004**, *126*, 3545−3550.

Scheme 2. Synthetic Path to the Oligo-phenylenevinylenediimide ImPV

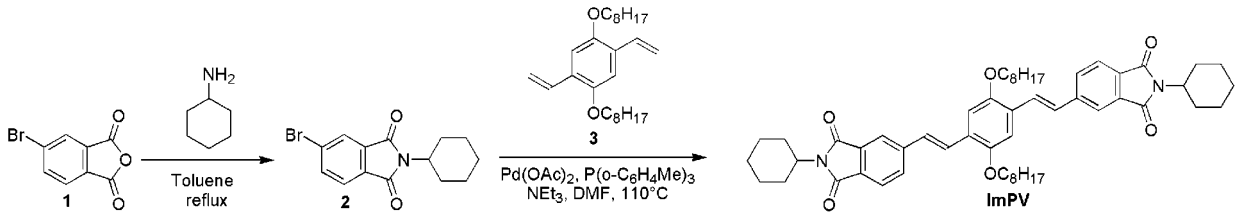

Substituted OPVs exhibit very promising properties in the field of light-emitting diodes (LED), and their encapsulation in silica matrixes improves their optical properties.[17] Most of studies have been done on bulk hybrid materials. Such approaches are not representative of the hypothetical material use as a thin film in a LED.

Recently, Dantas de Morais et al. have shown the ability of the sol−gel technique to produce multilayer devices comprising two or three hybrid layers exhibiting different functionalities.[18] Mono-functionalized molecules were copolymerized with tetraethoxysilane (TEOS) used as cross-linking agent. They demonstrated the electroluminescent properties of sol−gel materials by manufacturing hybrid organic−inorganic LED. But, the dispersion of the electroluminescent moiety in the silica matrix emerging from the hydrolysis of the TEOS did not allow studying the influence of the sol−gel process on the supramolecular organization of the chromophor. In a same way, Müllen et al. reported the fabrication of electroluminescent devices based on perylene-doped sol−gel layers.[19] The study of the influence of the sol−gel process on the supramolecular organization and on the optoelectronic properties could not be done since the fluorescent perylene dye was embedded in a hybrid sol−gel matrix by the adjunction of TEOS.

Here, the objective was to design and synthesize electroluminescent hybrid organic−inorganic materials by the sol−gel process applied to a bifunctionalized silane based on ImPV without TEOS in order to study the impact of the formation of the silica network. Effects on the quality of the thin films and on the electrooptical properties of the precursor subjected or not to the sol−gel process were investigated. For that purpose, we report, the synthesis of a new phenylenevinylenediimide silsesquioxane and the study of spin-coated thin films of the pure silane precursor subjected or not to the sol−gel process.

Results and Discussion

The Cyclohexyle Fragment as the Structure-Directing Agent. ImPV was synthesized in two steps from the 4-bromophthalic anhydride **1**. In a first step, the cyclohexylamine and the 4-bromophthalic anhydride **1** were condensed in refluxing toluene under a Dean−Stark trap to afford the corresponding halogenated cyclohexylphthalimide **2**[3] (Scheme 2). Finally, **2** readily underwent coupling reaction with the conjugated 1,4-divinyl-2,5-bis(octyloxy)benzene **3** in the presence of a palladium catalyst. The Heck reaction was carried out in dry *N*,*N*-dimethylformamide at 100 °C in the presence of $Pd(OAc)_2$ and of $P(o\text{-}C_6H_4Me)_3$. Yellow needles of ImPV were simply isolated through a filtration since they crystallized during the reaction mixture cooling. This new chromophore is highly soluble in common organic solvents, highly fluorescent, and emits greenish blue light with a fluorescence quantum yield of 70% when irradiated at 425 nm in tetrahydrofuran (THF) [$\lambda_{abs\_max} = 425$ nm; $\lambda_{em\_max} = 515$ nm ($\lambda_{ex} = 425$ nm), $\Phi_{flmPV} = 0.70$].

Upon deposition of a film of ImPV from a THF solution on a glass plate, the absorbance was red-shifted to 441 nm (Supporting Information). These small red shifts in absorbance and fluorescence maxima are consistent with an exciton coupling of the aromatic units due to the formation of J-aggregates. This agrees with the steric hindrance introduced by the cyclohexyl fragments.

Indeed, the steric contribution of the cyclohexyl fragment to the supramolecular arrangement of ImPV was determined by X-ray diffraction. Crystals obtained were suitable to record microdiffraction patterns at the Microfocus Beamline ID23-2 (European Synchrotron Radiation Facility − ESRF, Grenoble). ImPV crystallizes in a monoclinic system with a *C*2/*c* space group. One independent half-molecule is located on an inversion center (Figure 2a).

As attested by the single-crystal structure, the crystallization of ImPV afforded the all-trans compound. The three benzene rings (A, B, and B′) linked by double bonds are mostly coplanar with a dihedral angle C(7)−C(6)−C(3)−C(2) 11.08(3)°. Alternatively, the cyclohexyl fragments (in a chair conformation) are lying perpendicularly to the plane defined by the aromatic rings with a dihedral angle C(13)−N(1)−C(14)−C(15) 63.10(3)°. This conformation and the steric hindrance introduced by the cyclohexyl units result in a J-type organization of ImPV in the solid state (Figure 2b). In the crystal, J-stacks organized in layers separated by alkyl side chains along the *a* axis are formed (see Supporting Information).

To get information on charge injection, electrochemical measurements have been performed and compared to a highly studied light emitting polymer, poly[2-methoxy-5(2′-ethylhexoxy)-1,4-phenylenevinylene], known as MEH-PPV. MEH-PPV has been extensively demonstrated as a promising light-emitting polymer in the past 10 years.[20] ImPV exhibited a pseudo-reversible wave under cathodic sweep, and the reduction took place at −1.34 V ($E_{LUMO} = -3.06$ eV) versus saturated calomel electrode (vs SCE) which was higher than that of MEH-PPV (−1.52 V i.e. $E_{LUMO\ MEH-PPV} = -2.88$ eV).[21] The reduction process for a conjugated molecule in an electrochemical cell is

(16) Corriu, R. J. P.; Hesemann, P.; Lanneau, G. F. *Chem. Commun*. **1996**, 1845−1846.
(17) Prasad, P. N. *Mater. Res. Soc. Symp. Proc*. **1990**, *180*, 741−746.
(18) Dantas de Morais, T.; Chaput, F.; Lahlil, K.; Boilot, J-P. *Adv. Mater*. **1999**, *11*, 107−112.
(19) Schneider, M.; Hagen, J.; Haarer, D.; Müllen, K. *Adv. Mater*. **2000**, *12*, 351−354.
(20) (a) Yu, G.; Zhang, C.; Heeger, A. J. *Appl. Phys. Lett.* **1994**, *64*, 1540−1542. (b) Burroughes, J. H.; Bradley, D. D. C.; Brown, A. R.; Marks, R. N.; Mackay, K.; Friend, R. H.; Burn, P. L.; Holmes, A. B. *Nature* **1990**, *347*, 539−541.
(21) (a) Campbell, I. H.; Davids, P. S.; Smith, D. L.; Barashkov, N. N.; Ferraris, J. P. *Appl. Phys. Lett.* **1998**, *72*, 1863−1865. (b) Scott, J. C.; Brock, P. J.; Salem, J. R.; Ramos, S.; Mallarias, G. G.; Carter, S. A.; Bozano, L. *Synth. Met.* **2000**, *111*−*112*, 289−293.

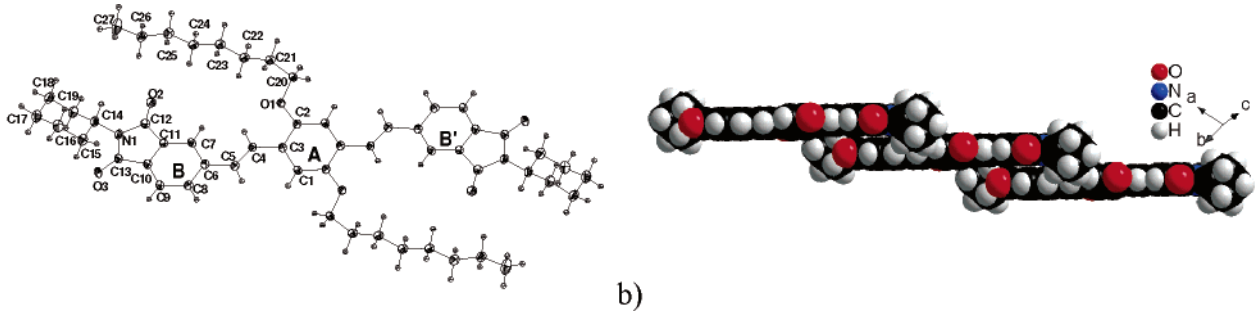

Figure 2. Crystal structure recorded on a single crystal of ImPV: (a) anisotropic displacement parameters are drawn at the 50% probability level. (b) J-stacks running along the *a* axis (octyl chains were omitted for clarity).

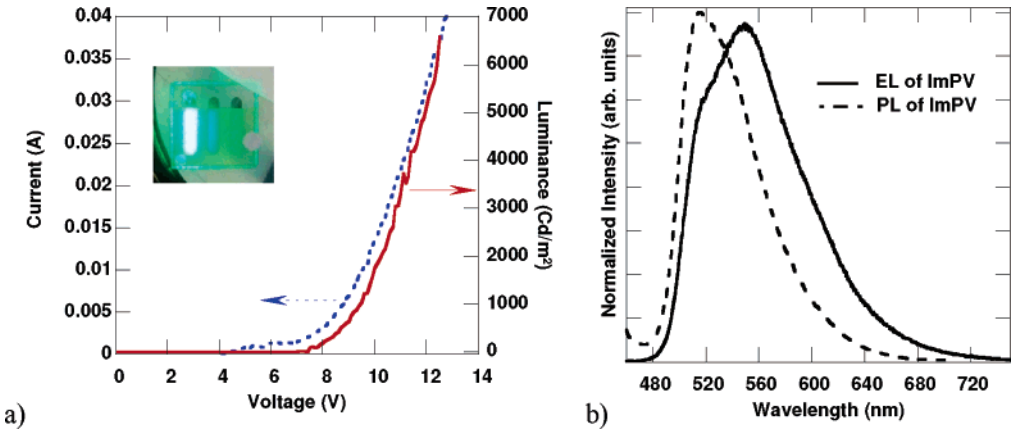

Figure 3. ITO/PEDOT-PSS/ImPV (50 nm)/LiF/Al device. (a) IVL curves (inset shows a picture of an operated OLED pixel). (b) Electroluminescence (EL) and photoluminescence (PL) spectra of ImPV. PL spectrum has been taken in the solid state with an excitation wavelength of 441 nm.

related to the electron capture ability. Therefore, it is reasonable to affirm that the ImPV has a higher electron affinity than MEH-PPV, owing to the introduction of the electron-withdrawing imido groups. The oxidation process exhibits an irreversible wave, and the onset potential of oxidation is located at 1.07 V vs SCE ($E_{HOMO} = -5.47$ eV). The oxidation process for a conjugated molecule in an electrochemical cell is closely related to the removal of electrons from the HOMO of the material. This value is higher than that of 0.59 V for MEH-PPV ($E_{HOMO\ MEH-PPV} = -4.99$ eV).[21] A higher oxidation potential of ImPV and an irreversible anodic wave present a barrier to hole injection. This may solve the problem of imbalanced charge transport of MEH-PPV based PLED, in which hole transport is much more effective than electron transport. The electrochemical band gap (E_g^{EC}), calculated from cyclic voltammetry data ($E^{ox}_{on} - E^{red}_{on}$), is about 2.41 eV, somewhat in good accordance with the optical band gap (E_g^{opt}) estimated from the onset absorption of ImPV ($\lambda_{onset} = 490$ nm), which corresponds to 2.53 eV.

Taking into account HOMO (−5.47 eV) and LUMO (−3.06 eV) level positions, an electroluminescent diode based on ImPV was fabricated using a system ITO/PEDOT-PSS (−5 eV) as an anode and LiF/Al as a cathode. The structure of the device included a layer of indium tin oxide (ITO) which is the commonly used transparent anode for such applications with a sheet resistance of approximately 17 Ω/□. This substrate underwent a wet cleaning procedure of successive 30 min ultrasonic baths in trichloroethylene, ethanol, and deionized water at room temperature. The substrates subsequently underwent a UV-ozone treatment. Then, a layer of poly(styrene sulfonate)-doped poly(3,4-ethylenedioxythiophene) (PEDOT-PSS) was spun, from a 3 wt % water dispersion at 5000 rpm to form a 50 nm thick layer. This conducting polymer layer was cured at 80 °C under primary rotary pump vacuum for 1 h. This layer improves hole injection from the ITO to the HOMO level of the organic material and increases the performances of the device.[22] Then, the active layer of ImPV was thermally evaporated under vacuum (ca. 10^{-6} mbar) at a low deposition rate of 0.1 nm s^{-1}. The deposited thickness (50 nm) was monitored using a piezoelectric balance setup inside the vacuum chamber close to the substrate holder. Thicknesses were checked with a Tencor AS-IQ profilometer. Bilayer cathodes of lithium fluoride LiF (∼1 nm thick) and aluminum Al (∼150 nm thick) were then sublimed under secondary vacuum through a shadow mask. All investigated devices have an active area of 10 mm^2. Samples were then stored and characterized under inert atmosphere in a nitrogen glovebox (O_2 and H_2O < 1 ppm). Contacts were taken using a prober (Karl Suss PM5). Current−voltage−luminance (IVL) curves were measured using a Keithley 2400 Sourcemeter coupled to a photodiode calibrated with a Minolta *CS-100* luminancemeter. Electroluminescence spectra (EL) were investigated using an Ocean Optics HR2000 Spectrometer.

Figure 3 shows current−voltage−luminance characteristics (IVL) of a device based on ImPV as a luminescent material. OLED based on ImPV exhibited very good performances. Luminances reach 6200 Cd/m^2 at 12 V with an onset voltage of 6.0V, a quantum efficiency maximum of 1.78 Cd/A, and a luminous efficiency maximum of 0.46 lm/W at 4000 Cd/m^2 (see Supporting Information). The electroluminescence (EL) spectrum has been measured and found centered at 545 nm with a onset at $\lambda_{onset} = 495$ nm. This EL spectrum is in good agreement

(22) Wantz, G.; Hirsch, L.; Huby, N.; Vignau, L.; Silvain, J. F.; Barrière A.-S.; Parneix, J.-P. *Thin Solid Films* **2005**, *485*, 247−251.

Scheme 3. Synthetic Path to the Phenylenevinylenediimide Silsesquioxane Precursor **6**

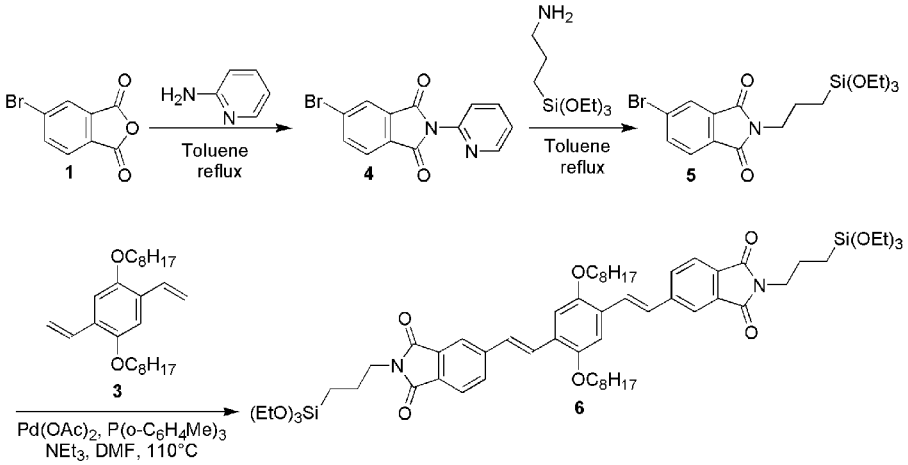

with HOMO and LUMO level positions deduced by cyclic voltammetry since it provides a band gap width of 2.50 eV. The observed light is pale green. The chromatic coordinates calculated from the EL spectra are reported at $x = 0.41/y = 0.57$ following the CIE-1964 chromaticity diagram. A red-shift is observed on the electroluminescence spectrum of ImPV (Figure 3b, $\Delta\lambda = 30$ nm) compared to the photoluminescence spectrum. Such an effect related to built-in electric fields was already observed.[23] Moreover, when operating these devices as photovoltaic cells under 470 nm irradiation using a 6 mW blue GaN light emitting diode, no photocurrent has been observed.

The good efficiencies exhibited by the devices based on a single layer of ImPV are the result of the J-aggregation of chromophores directed by the bulky cyclohexyl fragments. Modifications of this aggregation trend should modify its optical properties. Since the supramolecular organization of ImPV is the result of combined steric effects with π-stacking and van der Waals interactions, the only way to control it resides in the chemical modification of ImPV. This could be envisaged via the imide function. Indeed, any amine could be condensed to the 4-bromophthalic anhydride to furnish the reactive halogenated imide. The 3-aminopropyl)triethoxysilane was selected as a modifiable bulky amine to induce a J-aggregation and to offer the possibility to reach an H-aggregation upon its hydrolyze-polycondensation by the sol−gel process.

The Triethoxysilyle Fragment as the Structure-Directing Agent. The synthesis of the sol−gel processable precursor **6** is accomplished by introducing the triethoxysilyle group through a transimidation[24] from the imidopyridine derivative **4** rather than the direct addition of the 3-aminopropyl)triethoxysilane on the 4-bromophthalic anhydride **1** (Scheme 3).

Although such direct syntheses of [(trialkoxysilyl)propyl]-imides have been reported,[24] they often result in the premature hydrolysis and condensation of silylated monomers since the imide formation releases 1 equiv of water.[25] The halogenated [(triethoxysilyl)propyl]imide **5** was isolated in two steps from the anhydride **1**. In a first step, the 2-aminopyridine and the anhydride **1** were condensed in refluxing toluene under a Dean−Stark trap to afford **4** after a recrystallization of the crude product. The transimidation of the imidopyridine by the 3-aminopropyl)triethoxysilane afforded **5** which was isolated by column chromatography on silica gel with an overall yield of 60%. Finally, **5** readily underwent a coupling reaction with the conjugated 1,4-divinyl-2,5-bis(octyloxy)benzene **3** in the presence of a palladium catalyst. The Heck reaction was carried out in dry *N*,*N*-dimethylformamide in the presence of $Pd(OAc)_2$ and $P(o\text{-}C_6H_4Me)_3$. The sol−gel processable conjugated segment **6** was purified by column chromatography on silica gel. An additional recrystallization from ethanol afforded **6** as small red needles in 65% yield. This new silylated precursor is highly soluble in common organic solvents, highly fluorescent, and emits greenish-blue light with a solution fluorescence quantum yield of 70% when irradiated at 425 nm in tetrahydrofuran [THF, $\lambda_{abs\_max} = 432$ nm; $\lambda_{em\_max} = 530$ nm ($\lambda_{ex} = 432$ nm), $\Phi_{f6} = 0.70$].

Upon deposition of a THF solution of **6** on a glass plate, the absorbance is red-shifted to 466 nm. The large shifts in absorbance and fluorescence maxima are consistent with exciton coupling of the aromatic units due to the formation of J-aggregates. Spectral shifts ($\Delta\lambda = 30$ nm) higher than those of ImPV ($\Delta\lambda = 15$ nm) are consistent with the fact that triethoxysilane groups [$Si(OEt)_3$] are bigger than cyclohexyle fragments (see Supporting Information).

Further insight into the supramolecular arrangement was obtained by X-ray diffraction. Recrystallization of **6** in ethanol furnished small needles and microdiffraction patterns were recorded at the Microfocus Beamline ID23-1. **6** crystallizes in a monoclinic system with a $P2_1/c$ space group. One independent half-molecule is located on an inversion center (Figure 4a).

The thermal motions result in a splitting of the triethoxysilane fragment on two positions. Their positions have been refined according to a model of disorder. As in the case of ImPV, the recrystallization of **6** afforded the all-trans compound. The three benzene rings (A, B, and B′) linked by double bonds are coplanar with a small dihedral angle C(11)−C(10)−C(14)−C(19) 0.20(3)°. Conversely, the propyltriethoxysilane fragments are lying on each side of the plane defined by the aromatic rings, resulting in a chair conformation of the whole molecule with an angle C(23)−C(22)−N(2) 112.09(2)°.

This conformation and the steric hindrance introduced by the triethoxysilane units result in a J-type organization of **6** in the

(23) (a) Campbell, I. H.; Hagler, T. W.; Smith, D. L.; Ferraris, J. P. *Phys. Rev. Lett.* **1996**, *76*, 1900−1903. (b) Bolognesi, A.; Bajo, G.; Paloheimo, J.; Östergärd, T.; Stubb, H. *Adv. Mater.* **1997**, *9*, 121−124.
(24) Wengrovius, J. H.; Powell, V. M.; Webb, J. L. *J. Org. Chem.* **1994**, *59*, 2813−2818.
(25) Lo, S. J.; Swihard, T. J.; Ward, A. H. U.S. Patents 4,906,399 and 4,956,-472, Dow Corning Corp., 1990.

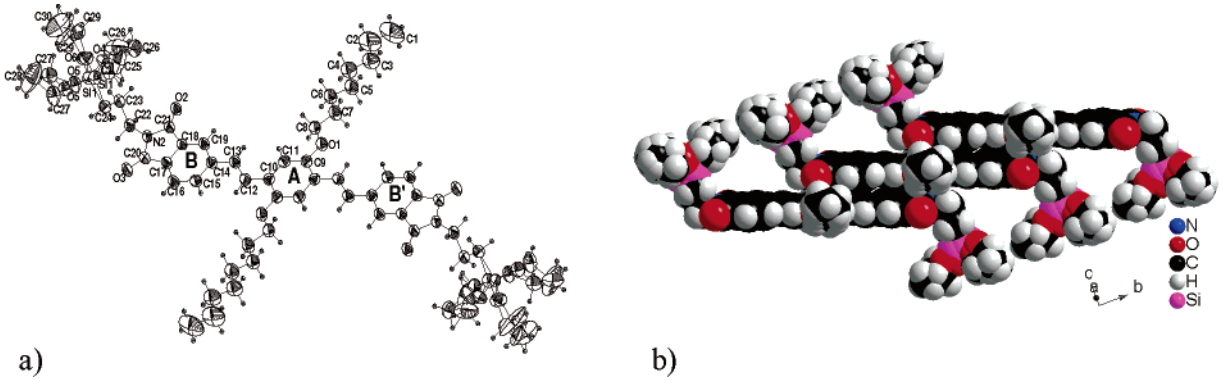

Figure 4. Crystal structure recorded on a single crystal of **6**: (a) anisotropic displacement parameters are drawn at the 50% probability level; (b) J-stacks running along the *b* axis.

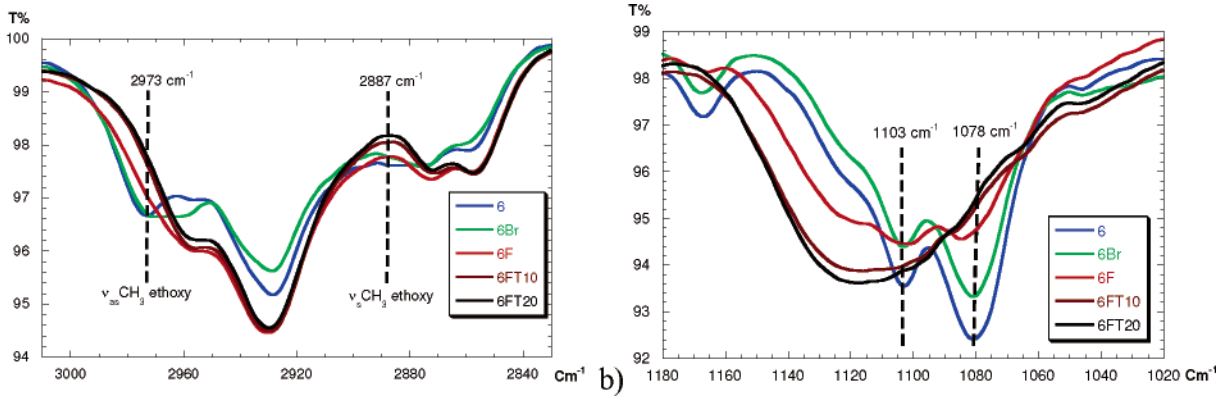

Figure 5. Infrared spectra of **6**, **6F**, and **6Br** films on silicon wafers: (a) spectral region from 2840 to 3000 cm^{-1}; (b) spectral region from 1020 to 1180 cm^{-1}.

solid (Figure 4b). In the crystal, **6** forms J-stacks organized in layers separated by alkyl side chains along the *a* axis (see Supporting Information).

Tuning the Supramolecular Organization by the Sol−gel Process. The contribution of the sol−gel process was revealed by the comparison of thin films obtained from THF solutions of **6** with or without catalyst. **6** was hydrolyzed by the sol−gel process using tetrabutylamonium fluoride (TBAF) as the catalyst. A solution of **6** in THF (25 mg·mL^{-1}, 23 mmol·L^{-1}), 0.5 equiv of TBAF, and 6 equiv of H_2O was deposited by spin-coating on different substrates before its gelation which took place within 10 min. Glass plates were used for the study of the optical properties, and silicon wafers for the studies related to the infrared spectroscopy, X-ray diffraction, and atomic force microscopy analyses. Films obtained by the sol−gel process using TBAF will be noted **6F**. The hydrolysis poly-condensation process can be monitored by infrared spectroscopy (Figure 5). During this chemical modification, the ethoxy groups of **6** are eliminated while Si−O−Si bonds are created. This transformation can be monitored from the band intensity of the asymmetric ($\nu_{as}CH_3$) and symmetric (ν_sCH_3) stretching vibrations of the CH_3 respectively at 2973 and 2887 cm^{-1} (Figure 5a). On the FTIR spectrum of **6F**, the intensity of these vibrations are lowered which is significant of the hydrolysis of the Si−OEt bonds. The hydrolysis of the thin film **6F** is complete after 20 min of 100 °C heating under air atmospheric pressure.

These bands have completely disappeared on the spectrum related to the annealed film **6FT20** (**6F** after 20 min of thermal treatment). The influence of the cation of the tetrabutylammonium salt on the physical and morphological properties of the films has been estimated using tetrabutylammonium bromide instead of tetrabutylammonium fluoride since the lower nucleophily of the bromide inhibits the hydrolyses−polycondensation process. In this case, films are noted **6Br**. As expected, no hydrolysis was observed when TBABr was used. FTIR spectra of **6F**, **6FT20**, and **6Br** showed two supplementary vibrations bands observed at 2960 and 2870 cm^{-1} which are attributed to the asymmetric and symmetric stretching vibrations of the CH_3 of the alkyl fragments of the $(Bu)_4N^+$ cation.

In a same way, the formation of the Si−O−Si network can be followed by the decrease of the band intensity of the asymmetric (ν_{as}Si−O−CH_2) and the symmetric (ν_sSi−O−CH_2) stretching vibrations of the Si−O−CH_2 bond, respectively observed at 1103 and 1078 cm^{-1} (Figure 5b) and the appearance of a broad band from 1060 to 1160 cm^{-1} corresponding to the asymmetric and symmetric stretching vibrations of the various Si−O−Si bonds of the silicate network. The condensation is complete after 20 min of thermal treatment. This was confirmed by the stability of the film **6FT20** faced with solvents washings and the absence of the νO−H of the water and the νSiO−H around 3400 cm^{-1} on its FTIR spectrum (Supporting Information).

The optical properties of the different thin films on glass plate revealed that the hydrolysis−condensation process resulted in a modification of the supramolecular organization of **6** in the solid state. Indeed, **6** on glass is characterized by an absorption maximum at 466 nm (Figure 6).

This maximum is hypsochromically shifted to 431 nm when **6** is subjected to a sol−gel process using TBAF in THF and spin-coated on glass to give **6F**. A proof that **6F** optical behavior

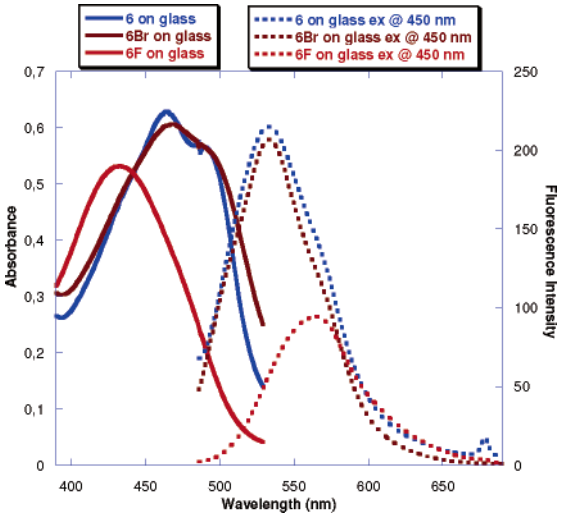

Figure 6. UV-vis and emission spectra of films of **6**, **6F**, and **6Br** on glass.

Scheme 4. Modelization of the Organization Changes from a Thin Film of **6** to a Thin Film of **6F** Due to the Sol−Gel Process: From a J-Aggregation to an H-Aggregation

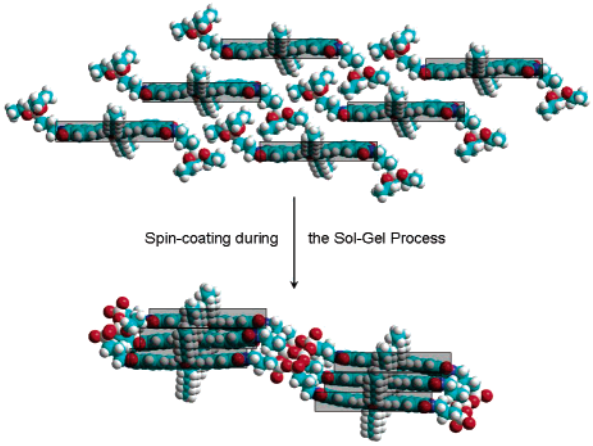

resulted from cross-linking of the siloxanes is given by the blank test using TBABr instead of TBAF which revealed no change in the absorption maximum of **6Br**. A comparison of the fluorescence spectra showed a different trend. In contrast to the absorption spectra, the fluorescence maxima reflected a bathochromic shift from 534 nm for **6** to 563 nm for **6F**. Again, **6Br** showed the same fluorescence properties as **6**. The changes of the electronic spectra can be attributed to a different aggregation behavior of the chromophores in relation with their confinement in a silicate network (**6F**) or not (**6**). The spectroscopic behavior observed for confined **6F** (blue-shifted absorption, red-shifted and quenched emission) can be attributed to an H-aggregation,[26] which is reasonable to expect from an anticipated "card pack" orientation of the distyrylbenzeneimide chromophores in the compressed silicate network (Scheme 4). A possible formation of 2D aggregates is less likely since H-aggregates should be separated from each other by long alkyl chains preventing exciton coupling. As already established from the X-ray diffraction analyses, the bulky triethoxysilane fragments of **6** are responsible of a J-type aggregation. (Figure 4).

Moreover, the formation of the silicate network supports a face to face organization of the chromophores in an H-type aggregation. It's known that going from a J-aggregation to an H-aggregation reduces the fluorescence quantum yields in favor of the intermolecular overlaps.[27,28] In the case of the fluoride ion catalyzed hydrolysis, it is difficult to compare fluorescence solid-state quantum yields since **6** and **6F** stand on two different substrates. This problem can be circumvented by following the hydrolysis−polycondensation of **6** deposited on a glass plate catalyzed by HCl vapors (see Supporting Information).[29] Indeed, infrared, UV−vis, and fluorescence monitoring of a glass plate spin-coated with **6** exposed to vapors of concentrated HCl showed that the fluorescence intensity of **6** decreases during the hydrolysis-polycondensation process and 56% of the fluorescence intensity is lost when **6** is totally converted in **6Cl** ($\Phi_{\text{fsolide}\mathbf{6Cl}} = 0.44\ \Phi_{\text{fsolide}\mathbf{6}}$). Additionally, the thermal treatment of **6F** for 20 min at 100 °C completes the condensation process and gives a very stable and insoluble film. This step has a low influence on the absorption (1.3% lost) and emission intensities (10% lost). The slight blue-shift ($\Delta\lambda = 5$ nm) observed on the absorption spectrum of **6FT20** is significant of an increase of the H-aggregation, resulting of the contraction of the network. In a same way, the decrease of the fluorescence intensity is directly related to the H-aggregates known to reduce fluorescence quantum efficiencies.[10,30] As observed on the spectra of **6FT20washed**, no absorbance and fluorescence is lost during the different washings of the film with different solvents (methylene chloride, THF, acetone, etc.).

Further insight into the supramolecular arrangement of **6F** was obtained by X-ray diffraction data collected using a curve position sensitive detector INEL CPS-120 equipped with a Cu Kα ($\lambda = 1.542$ Å) source and a Ge monochromator. The X-ray diffraction of **6F** on silicon wafers (Supporting Information) suggested a highly uniform lamellar structure with intermolecular period of 19.8 Å ($q = 0.32$ Å^{-1}). In contrast, the X-ray diffraction pattern of **6**, on silicon wafer, implied a more complex out-of-plane supramolecular arrangement. Three different reflections related to periodicities of respectively 25.0 Å ($q = 0.25$ Å^{-1}), 21.2 Å ($q = 0.30$ Å^{-1}), and 19 Å ($q = 0.33$ Å^{-1}) were observed.

The sol−gel process allowed the formation of a very good quality thin film on glass or silicon wafer. Upon inspection of the topography of the spin-cast **6F** layer by atomic force microscopy (AFM) on tapping mode of a Dimension 3100 Veeco Instruments, one can observe several tens of nanometers long and 2 nm thick randomly lying plates, which indicate some degree of self-organization on the surface (Figure 7a).

The 2 nm thick nano-plates are directly related to the out-of-plane organization determined by X-ray diffraction with a period of 1.98 nm. These nano-plates, disposed parallel to the substrate, formed a very homogeneous surface (Figure 7b). The root-mean-square roughness ($R_{\text{rms}} = 1.8$ nm) of this film corresponds to the thickness of the nano-plates. In contrast, the morphology of the film obtained by spin-coating of **6** is extremely heterogeneous with an $R_{\text{rms}} = 20$ nm (Figure 7c and 7d).

(26) Kasha, M.; Rawls, H. R.; El-Bayoumi, M. A. *Pure Appl. Chem.* **1965**, *11*, 371−392.
(27) Schenning, A.; Jonkheijm, P.; Peeters, E.; Meijer, W. *J. Am. Chem. Soc.* **2001**, *123*, 409−416.
(28) Whitten, D. G. *Acc. Chem. Res.* **1993**, *26*, 502−509.
(29) Dautel, O. J.; Lère-Porte, J. P.; Moreau, J. E.; Wong Chi Man, M. *Chem. Commun.* **2003**, 2662−2663.
(30) (a) Manas, E. S.; Spano, F. C. *J. Chem. Phys.* **1998**, *109*, 8087−8101. (b) Varghese, R.; George, S.; Ajayaghosh, A. *Chem. Commun.* **2005**, 593−595.

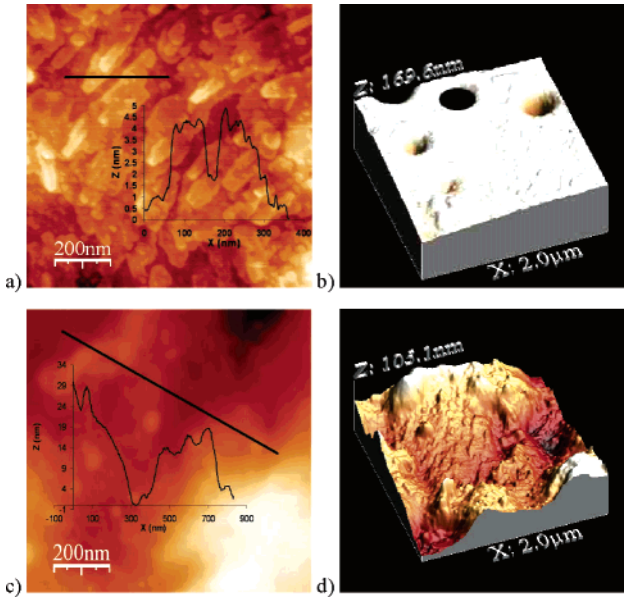

Figure 7. AFM (tapping mode) topography images and cross-sectional profiles for thin films of **6F** (a and b) and **6** (c and d) on silicon wafers.

To gain information on the charge injection, electrochemical measurements were performed. Figure 8a shows a full scan cyclic voltammograms for thin films of **6** and **6F** drop-cast on a platinum wire. **6F** was drop cast during the sol−gel process. Both compounds exhibit a pseudo-reversible wave under cathodic sweep and the reduction took place at −1.37 V vs SCE. Again, the new sol−gel processable monomer **6** has a higher electron affinity than MEH-PPV, owing to the introduction of the electron-withdrawing imido groups.

The oxidation process exhibits an irreversible wave when swept anodically and the onset potential of oxidation for **6** is located at 1.18 V vs SCE. **6F** exhibits a lower oxidation potential at 1.00 V (vs SCE). It's easier to inject holes in the HOMO of **6F** than that of **6**. The supramolecular reorganization optimizes the overlap between chromophores during the sol−gel process and improves the hole transport ability. As already deduced from the crystallographic analyses, these values of the oxidation potential showed that the J-type aggregation of **6** is more effective than that of ImPV. Indeed, the oxidation potential of ImPV (1.07 V) stands between **6F** (1.00 V) and **6** (1.18 V) values. The electrochemical band gaps (E_g^{EC}), calculated from cyclic voltammetry data ($E^{ox}_{on} - E^{red}_{on}$), are about 2.55 eV for **6** and 2.37 eV for **6F**, somewhat in good accordance with the optical band gap (E_g^{opt}) estimated from the onset absorption of thin film of **6** (2.45 eV, $\lambda_{onset} = 507$ nm) and **6F** (2.41 eV, $\lambda_{onset} = 513$ nm).

According to the experimental data given by UV−visible spectroscopies (absorption and emission), X-ray diffraction, microscopies (AFM, SEM, and TEM), and electrochemical measurements, **6** and **6F** should exhibit two different optoelectronic behaviors. The J-aggregation of **6** is in favor of its emission properties (solid-state fluorescence quantum yield) and the H-aggregation of **6F** supports its charge transport abilities (intermolecular overlaps). This has been illustrated by the fabrication of devices based on spin-coated films of **6** or **6F** sandwiched between two electrodes (Figure 8b). Following the experimental procedure described for ImPV-based diodes, the anode was ITO/PEDOT-PSS and the cathode was LiF (1 nm)/Al (150 nm).

From such electronic structures, it is believed that charge carrier injection may differ. The energetic barrier at the anodic interface is higher in OLED based on **6** than on **6F**. Hole injection is then easier in **6F**. At the cathodic interface, electron injection from LiF/Al is not limited by any energetic barrier in both cases. As a consequence, charge balance may be better in **6F** than in **6**. On this energetic basis, higher performances are expected from **6F**.

Figure 9a shows the measured luminance-voltage characteristics (LV) of devices based on **6** and on **6F**. OLEDs based on **6** exhibit low luminance levels for voltages lower than 30 V (10 Cd/m^2 @ 25 V) and the onset voltage is 5.5 V. A 21 V onset voltage is recorded with devices based on **6F** and smaller luminances are due to smaller current densities. Values of only 3.5 Cd/m^2 are observed at 30 V. Such very high applied voltages are consistent with poor performances of **6F**-based devices. As a consequence, the injection related data reported above are not sufficient to predict the performance of OLEDs. We believe that **6F** presents a poor ability to emit light because of the H-aggregation which induces quenching of luminescence. The use of **6** is therefore an interesting alternative to avoid H-aggregation and to significantly increase luminances. Interestingly, OLED made of **6Br**, which constituted the blank test, showed similar performances as **6** demonstrating that low performances of **6F** as light emitter arise from its supramolecular organization and not from the introduction of charged species in the thin-films.

Moreover, these diodes were operated as photovoltaic cells under irradiation from a simple blue GaN-based LED. Such photocurrent generators revealed the good charge carriers generation and transport abilities of **6F** (Figure 9b). Indeed, the illumination of the devices (**6** and **6F**) with such a lighting ($\lambda_{em} = 470$ nm) offered a photovoltaic effect (see IV curves in Supporting Information). Such a photoresponsive phenomenon has already been observed in a single layer structure (ITO/MEH-PPV/Ca) irradiated by a monochromatic light of 488 nm.[31] Considering the UV−vis spectra, ($\lambda_{abs\_max\mathbf{6}} = 466$ nm and $\lambda_{abs\_max\mathbf{6F}} = 431$ nm), an excitation at $\lambda_{ex} = 470$ nm should exhibit better performances for **6** than **6F** in this setup (Supporting Information). Indeed, the absorption band of **6** perfectly matches the blue light used for the irradiation. However, the photocurrent generated by **6** (16 nA) under the blue light irradiation is twice smaller than that of **6F** (30 nA). These results agree with the H-aggregation of **6F** which is supposed to enhance the charge carrier mobility. Further experiments are under investigation in order to accurately evaluate the charge carrier mobilities.

One should note that the quality of thin-films of **6** has been improved by a sublimation process which afforded thin-films with similar quality of solution processed **6F** thin-films. Identical photocurrent levels were obtained for sublimated **6** but its light emitting performances were further improved which supports the preceding results. Luminances reach 450 Cd/m^2 at 15V with an onset voltage of 7.5V, a quantum efficiency maximum of 0.49 Cd/A, and a luminous efficiency maximum of 0.1 lm/W at 300 Cd/m^2 (Supporting Information). Substrates of ITO/

(31) Halls, J. J. M.; Pichler, K.; Friend, R. H.; Moratti, S. C.; Holmes, A. B. *Appl. Phys. Lett.* **1996**, *68*, 3120−3122.

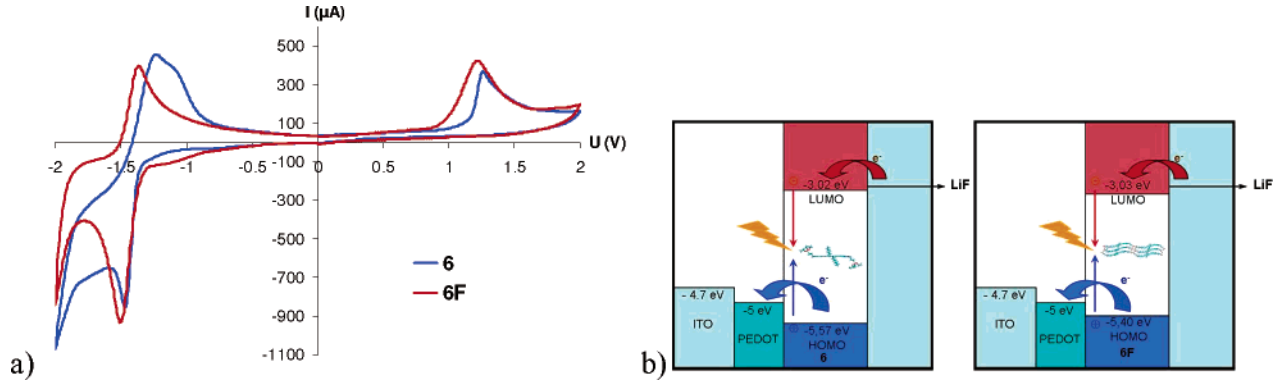

Figure 8. (a) Cyclic voltammograms of drop-cast films of **6** and **6F** on platinum wires in CH_3CN containing 0.1 mol L^{-1} of Bu_4NPF_6 as a supporting electrolyte at a scan rate of 100 mV s^{-1}, referenced vs SCE. (b) Energy level diagram of the devices fabricated with spin-coated films of **6** or **6F** (before contact).

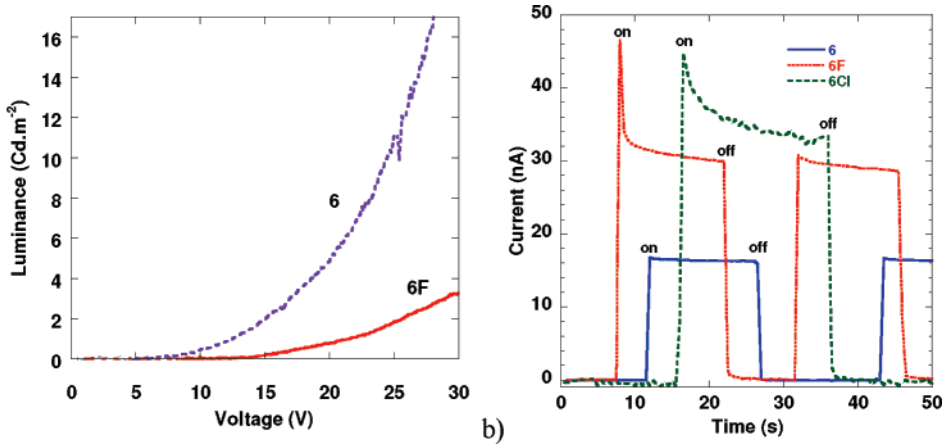

Figure 9. Performances of ITO/PEDOT-PSS/**6X** (50 nm thick)/LiF/Al devices. (a) LV curves. (b) Photocurrent generated by ITO/PEDOT-PSS/**6X** (50 nm-thick)/LiF/Al devices illuminated with a blue light (λ_{ex} = 470 nm). **6** (blue solid line), **6F** (red dotted line), and **6Cl** (green dashed line).

PEDOT-PSS/**6**(sublimated) were also exposed to vapors of concentrated HCl and gently rinsed with methanol to avoid PEDOT-PSS dilution. With such a procedure, devices based on **6Cl** have been made. As in the case of **6F**, light emission is highly reduced due to the π-stacking when operated as OLEDs. Under the blue illumination, devices based on **6Cl** present enhanced photocurrents compared to devices based on sublimated **6** (Figure 9b). One can note that **6Cl**-based cells exhibit higher photocurrent than **6F**-based ones. It is supposed that sublimation improves the quality of coatings in terms of roughness. As a consequence, sublimated devices present fewer defects and less leakage currents than wet processed ones. All these results are once again consistent with better charge transport properties due to the H-type aggregation of molecules compared to the J-type organization.

Conclusions

The synthesis of the sol−gel processable precursor **6** was accomplished by introducing the triethoxysilyl group through a transimidation from the imidopyridine derivative.

The shifts in absorbance and fluorescence maxima, observed upon deposition of a THF solution of **6** on a glass plate, are consistent with the supramolecular arrangement of **6** determined by X-ray microdiffraction: the all-trans conformation of the molecule and the steric hindrance introduced by the triethoxysilane units result in a J-type organization in the solid.

The interest of the sol−gel process was revealed by the comparison of thin films obtained from THF solutions of **6** with or without fluoride catalyst. The optical properties of the different thin films on glass plate revealed that the hydrolysis−condensation process resulted in a modification of the supramolecular organization. The changes of the electronic spectra have been attributed to a different aggregation behavior of the chromophores confined (**6F**) or not (**6**) in the silicate network. The spectroscopic behavior observed for **6F** (blue-shift in absorption, red-shift in fluorescence) could be attributed to an H-aggregation of the distyrylbenzeneimide chromophores in the compressed silicate network.

The sol−gel process allowed the formation of a very good quality thin film on glass or on silicon wafer. Upon inspection of the topography of the spin-cast **6F** layer by atomic force microscopy (AFM), randomly lying nano-plates were observed, which indicate some degree of self-organization on the surface.

The type of aggregation significantly affects the electronic properties of the material. This was demonstrated by means of electrochemical measurements and by the fabrication of optoelectronic devices operated as OLEDs or photovoltaic cells. Both exhibited high brightness and low photocurrents with the native precursor and almost no brightness and higher photocurrents with the sol−gel processed silsesquioxane. We believe that this approach of the control of electrooptical properties by the control of aggregation properties could be generalized to many labile and versatile structure-directing groups.

Acknowledgment. The authors gratefully acknowledge financial support from the "Ministère de la Recherche" and the

CNRS. We gratefully acknowledge the allocation of beam time for the experiment at the ID23 microfocus beamline at the European Synchrotron Radiation Facility-ESRF, Grenoble.

Supporting Information Available: Experimental procedure for the synthesis of ImPV, **4**, **5**, and **6.** Spectral data sets (NMR, UV−vis, fluorescence, FTIR, HRMS, elemental analyses) and ^{1}H and ^{13}C NMR spectra for ImPV, **4**, **5**, and **6**. Crystallographic information file (CIF) of ImPV and **6**. X-ray diffraction pattern of **6F** on silicon wafers. Detailed experiments for **6Cl**. Thin-films and devices fabrication methods. This material is available free of charge via the Internet at http://pubs.acs.org. .

JA058680Z